Article

Cell Reports

Sex-Specific Features of Microglia from Adult Mice

Graphical Abstract

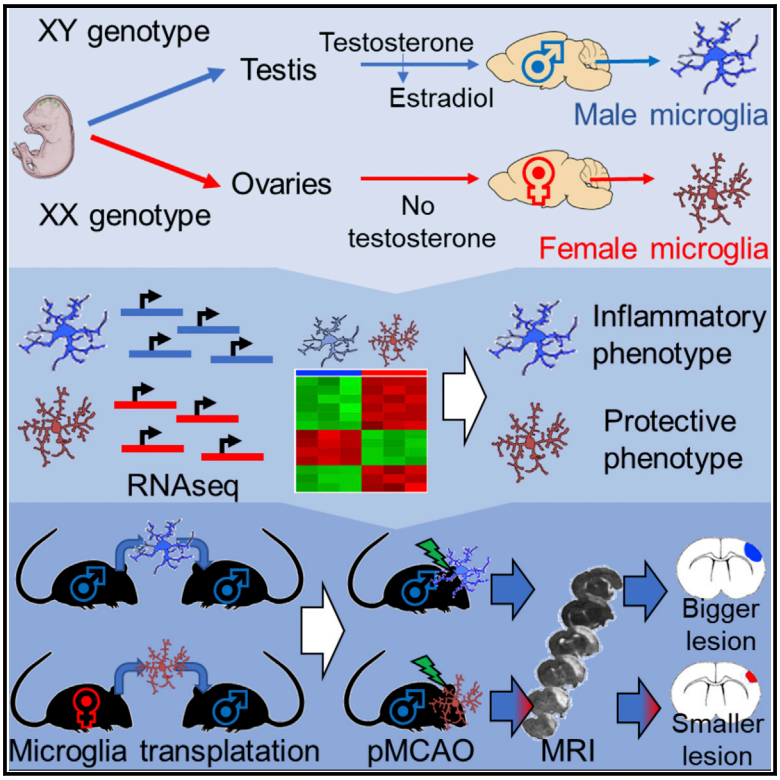

Authors

Alessandro Villa, Paolo Gelosa, Laura Castiglioni, ..., Luigi Sironi, Elisabetta Vegeto, Adriana Maggi

Correspondence

adriana.maggi@unimi.it

In Brief

Villa et al. find significant differences in the transcriptomes of microglia isolated from the brains of healthy adult male and female mice. They find that microglia from female mice are neuroprotective and that they retain this functional ability when transferred into the brains of male mice.

Highlights

- Transcriptome sequencing indicates sexual differentiation in adult murine microglia
- Female microglia show a neuroprotective phenotype, independent from hormonal cues
- Female microglia phenotype is retained after transfer into male brains
- The presence of female microglia protects male brains from ischemic stroke

Villa et al., 2018, Cell Reports *23*, 3501–3511
June 19, 2018
https://doi.org/10.1016/j.celrep.2018.05.048

CellPress

Cell Reports
Article

Sex-Specific Features of Microglia from Adult Mice

Alessandro Villa,[1,2] Paolo Gelosa,[3] Laura Castiglioni,[2] Mauro Cimino,[4] Nicoletta Rizzi,[2] Giovanna Pepe,[1,2] Federica Lolli,[2] Elena Marcello,[2] Luigi Sironi,[2,3] Elisabetta Vegeto,[1,2] and Adriana Maggi[1,2,5,*]
[1]Center of Excellence on Neurodegenerative Diseases of the University of Milan, Milan 20133, Italy
[2]Department of Pharmacological and Biomolecular Sciences, University of Milan, Milan 20133, Italy
[3]Centro Cardiologico Monzino IRCCS, Milan 20138, Italy
[4]Department of Biomolecular Sciences, University of Urbino, Urbino 61029, Italy
[5]Lead Contact
*Correspondence: adriana.maggi@unimi.it
https://doi.org/10.1016/j.celrep.2018.05.048

SUMMARY

Sex has a role in the incidence and outcome of neurological illnesses, also influencing the response to treatments. Neuroinflammation is involved in the onset and progression of several neurological diseases, and the fact that estrogens have anti-inflammatory activity suggests that these hormones may be a determinant in the sex-dependent manifestation of brain pathologies. We describe significant differences in the transcriptome of adult male and female microglia, possibly originating from perinatal exposure to sex steroids. Microglia isolated from adult brains maintain the sex-specific features when put in culture or transplanted in the brain of the opposite sex. Female microglia are neuroprotective because they restrict the damage caused by acute focal cerebral ischemia. This study therefore provides insight into a distinct perspective on the mechanisms underscoring a sexual bias in the susceptibility to brain diseases.

INTRODUCTION

Investigation into the role of microglia, the myeloid cells that reside in the CNS, has begun to receive intense interest, unravelling the complexity of the effects that these cells have on neural functions and establishing their major role in the development and life-long maintenance of brain homeostasis (Kierdorf and Prinz, 2017; Prinz and Priller, 2014; Salter and Stevens, 2017).

During development, microglia have been shown to influence neurodevelopmental processes such as axon guidance, neurite growth, and synaptic pruning (Kettenmann et al., 2013; Schafer et al., 2013; Wu et al., 2015), and to follow a precise and coordinated transcriptional program (Matcovitch-Natan et al., 2016). In addition, it has been demonstrated that microglia participate in the process of brain masculinization induced by the neonatal surge of male gonadal activity (Lenz et al., 2013); this process organizes brain architecture by structuring neuronal circuits to be activated by sexual functions after puberty (Arnold and Gorski, 1984; MacLusky and Naftolin, 1981). In adults, microglia are the first line of protection against noxious stimuli such as stress and pathogenic insults, and they maintain healthy brain function by pruning synapses (Kettenmann et al., 2013; Wu et al., 2015), clearing debris (Neumann et al., 2009), and synthesizing growth and repair factors (Hu et al., 2015). In spite of this, prolonged microglia stimulation may lead to neuronal damage. Indeed, several recent studies have highlighted the involvement of microglia and neuroinflammation in the manifestation of major neurological and neuropsychiatric diseases.

The finding that these cells are responsive to estrogens and that their immune functions and inflammatory response are significantly mitigated by estrogens (Vegeto et al., 2001) may point to a role of this hormone in determining the sex-specific prevalence, onset, and course of numerous brain diseases (Vegeto et al., 2002; Villa et al., 2016). Furthermore, increasing evidence suggests that neurological disorders have their roots in diversions from a normal developmental trajectory, and disturbances and a loss of microglial function have been associated with the onset of brain diseases (Prinz and Priller, 2014). Considering the role of microglia in brain sexual differentiation, it could be hypothesized that the effects of estrogens during brain differentiation may induce permanent effects in microglia, enabling these cells to contribute to sex-related manifestation of brain diseases (Villa et al., 2016).

The aim of the present study was to identify the differences in the transcriptome of male and female microglia isolated from adult healthy mice and to verify the extent to which microglia sex differences might affect the progress of pathologies where these immune cells play a major role.

RESULTS

RNA-Sequencing Highlights Sex Differences in Adult Microglia

To study the expression profile of male and female microglia, we took advantage of a recently developed methodology to isolate these cells at high level of purity from adult brain (Hanamsagar et al., 2017; Pepe et al., 2014) (Figure S1A–S1D). To avoid the variability related to rearing, environment, or diets affecting the metabolism and the microbiome, both well-known regulators of the brain immune system (Hooper et al., 2012), care was taken to match the mice in terms of age and to take the same number of males and females from each of the litters utilized in the study. To limit any circadian influence and facilitate the analysis of the phase of the cycle, in all experiments, animals were euthanized

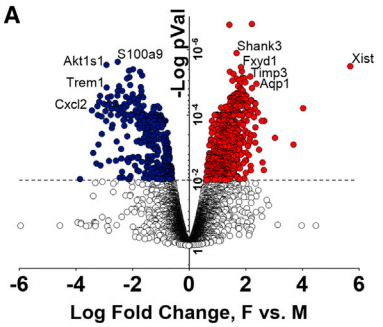

B

	GO term	pVal	TFs	pVal
MALES	Inflammatory response	3.78E-18	NF-κB	4.20E-04
	Leukocyte migration	6.11E-14	RUNX1	8.27E-04
	Regulation of response to wounding	2.84E-12	FOXM1	1.68E-03
	Chemotaxis	9.86E-12	GATA2	4.00E-02
	Reg. of cytokine production	4.48E-11		
FEMALES	Movement of Cell	1.10E-16	NANOG	7.97E-07
	Nervous System Development	1.11E-15	TCF3	3.79E-05
	Cell Migration	1.38E-15	ELK3	2.87E-04
	Vasculature Development	7.60E-08	ESR1	9.02E-03
	Anatomical Structure Formation	5.54E-07	EZH2	7.36E-03
	Actin Cytoskeleton Organization	6.91E-07	SOX9	7.94E-03

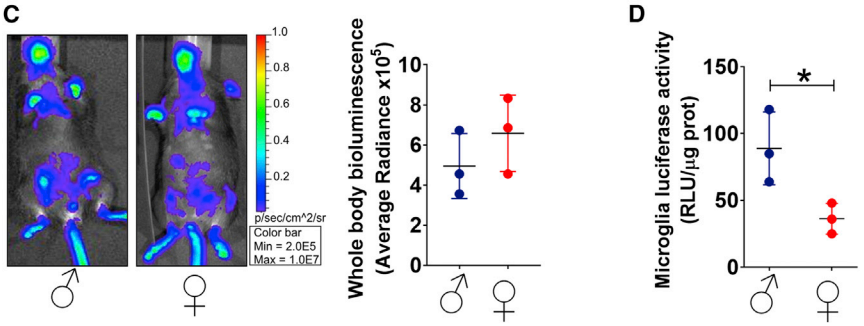

Figure 1. Microglia Transcriptome in the Male and Female Mouse Brain

(A) Volcano plot of RNA-seq data obtained from microglia isolated from male and female adult C57BL/6 mice. Analyses were conducted on two pools of six brains each, a total of 12 males and 12 females. Blue dots represent genes for which RPKM values are significantly higher in males than in females (204 genes; $p < 0.01$ by Benjamini-Hochberg correction). Red dots represent genes for which RPKM values are significantly higher in females than in males (342 genes; $p < 0.01$).

(B) Gene Ontology and ChIP enrichment analysis (ChEA) transcription factor (TF) term enrichment analysis of transcripts with higher expression in male (blue) or in female (red) microglia.

(C) *In vivo* imaging of luciferase expression in male and female NFκB-*luc2* mice. Bioluminescence is measured ventrally and whole body, and the pseudocolors represent radiance (p/s/cm^2/sr). The image is representative of three independent measures on three mice per group per experiment. In the graph, each line corresponds to average radiance ± SEM.

(D) Luciferase activity measured in extracts of microglia isolated from the whole brains of male ($n = 3$) and female ($n = 3$) NFκB-*luc2* mice and expressed as relative luciferase units (RLUs) per microgram of proteins. Each sample was measured in triplicates. Lines represent the mean ± SEM of $n = 3$. *$p < 0.05$ by unpaired, two-tailed t test.

at the same hours (between 2:00 and 4:00 p.m.); females were at metestrus, a phase with low circulating estrogens.

The transcriptome was investigated by RNA sequencing (RNA-seq; RNA-seq data are available at the NCBI Sequence Read Archive: SRP104620). The RNAs were prepared from pools of 6 brains each: 2 pools were from males and 2 pools from females; thus, we utilized a total of 12 mice/sex. Mice were 12 weeks old. The transcriptional data were initially analyzed by AltAnalyze (Olsson et al., 2016) and mapped over the Tissue Fate Map to demonstrate the absence of contaminations from other neural cells. Indeed, the reads per kilobase million (RPKM) relative to biomarkers of neutrophils (*Ly6g*), B cells (*Cd19*), T cells (*Cd3–Cd8*), astrocytes (*Aldh1l1*), neurons (*Thy1*), and oligodendrocytes (*Olig1*) were found to be negligible with respect to the predominant microglia markers.

To determine the differently expressed genes (DEGs), we carried out the statistical analysis using the CuffDiff (Trapnell et al., 2012) software. By applying a threshold of 0.01 to the false discovery rate (FDR; Benjamini-Hochberg correction)-adjusted p values (pVal), we identified 546 DEGs (Figure 1A). The reliability of the RNA-seq results was tested on microglia isolated from 12 additional individuals (males, $n = 6$; females, $n = 6$); the results obtained with qPCR on a panel of 20 mRNAs randomly selected among those with sex-dependent and sex-independent expression demonstrated the reproducibility of the RNA-seq data (Figure S1E).

Next, to identify whether the DEGs could be associated with specific functional categories, we carried out a clustering analysis by Enrichr (Kuleshov et al., 2016). The majority of the 204 genes more expressed in males belonged to Gene Ontology classes associated with inflammatory processes, including regulation of cell migration and cytokine production (Figure 1B). Whole-genome molecular signature analysis of transcription factors (TFs) pointed to nuclear factor κB (NF-κB) as the TF most involved in the regulation of the DEG preferentially expressed in males, together with other TFs associated with inflammatory processes (RUNX1) (Kierdorf and Prinz, 2013), migration (FOXM1) (Balli et al., 2012), and negative regulation of neurogenesis (GATA2) (El Wakil et al., 2006). In contrast, no association with inflammation was found in the DEGs distinctive of female microglia that were grouped in ontogenies associated with morphogenesis, development, or cytoskeleton organization under the control of several TFs such as NANOG (Duan et al., 2013) and TCF3 (Miao et al., 2014), linked to the inhibition of inflammatory response and promotion of repair mechanisms (Duan et al., 2013; Miao et al., 2014), aside from the estrogen receptor alpha (ESR1) itself. The lack of a sex-dependent pro-inflammatory profile in macrophages isolated from the peritoneum of the male mice studied above (G.P. and E.V., unpublished data) suggested that this could be a microglia-specific feature.

The Inflammatory Phenotype of Male Microglia

We continued our study in the NFκB-*luc2* mouse model where the luciferase gene was under the control of an NF-κB-responsive synthetic promoter. This reporter mouse was specifically designed to study the inflammatory status in living cells and animals (Rizzi et al., 2017). Whole-body, *in vivo* imaging in

unstimulated conditions showed that the bioluminescence was comparable in siblings of the two sexes (n = 3) (Figure 1C); this result suggested a similar, generalized state of NF-κB transcriptional activation in males and females. However, when we measured luciferase activity in microglia purified from adult siblings of both sexes (n = 3), the luciferase activity was 2.4-fold higher in males (Figure 1D). These data supported our previous bioinformatic analysis by demonstrating that in male microglia NF-κB was transcriptionally activated, suggesting that male microglia cells were more poised to inflammatory reactions than female microglia. To substantiate the hypothesis of male microglia more prone to inflammatory activation, we further analyzed the RNA-seq data, focusing on a total of 95 genes that had been experimentally demonstrated to be targets of NF-κB and involved in immune or inflammatory responses (http://www.bu.edu/nf-kb/gene-resources/target-genes/).

Consistent with previous results, unbiased male-female comparative analysis (Figure 2A) showed that 79% of the 95 inflammatory genes were more expressed in males, and 34 of these genes were differentially expressed with a threshold of 0.05 applied to the FDR (Benjamini-Hochberg correction)-adjusted p values (clusters D, E, and F); of the remaining genes, 14% were expressed similarly in the two sexes (clusters B and C), and 7% were grouped in cluster A, possibly for having a trend to be more expressed in females.

Is Circulating 17β-Estradiol Responsible for Microglial Sex Differences?

To investigate the extent to which estrogens contributed to the sex differences observed in the NF-κB-regulated genes, we extended the analysis to the RNA-seq data on microglia isolated from mice ovariectomized (OVX) with or without estrogen replacement for 3 or 24 hr; such data were generated using groups of animals reared and treated in parallel with those described above. After ovariectomy, we observed a tendency toward a reduction in differences between the two sexes, with a generalized increase in the expression of the 95 NF-κB-driven genes (Figure 2A). However, Pearson analysis did not show significant changes when we did correlation analyses between the NF-κB genes expressed in OVX females/males (R = 0.9327) and cycling females/males (R = 0.8589), leading us to conclude that the gene expression of microglia was not significantly influenced by the lack of circulating sex steroids. Moreover, in the OVX mice, 17 of the original 34 DEGs were still found to be less expressed (with a threshold of 0.05 applied to the adjusted p values) than in males despite the lack of circulating estrogens; this finding pointed to the contribution of factors other than estrogens to the low expression of NF-κB-regulated genes. Hormone replacement induced a trend in the expression of these genes; hierarchical clustering (Pearson correlation, average linkage) identified three clusters of genes for which estrogen administration induced a rapid, transient increase (78%, clusters B, D, and F; Figure 2A), and a smaller group of genes (22%, clusters A, C, and E) showed the opposite trend, with a decreased expression after 3 hr of 17β-estradiol (E_2) treatment.

These findings suggested that the transcriptional differences of the NF-κB-regulated genes did not depend on estrogens in a predictable way, and that additional factors played a role in differentiating the male and female microglia transcriptomes.

To evaluate whether the sex differences observed were maintained *in vitro*, we prepared primary cultures of microglia isolated from adult male and female mice. To enable microglia to survive and to preserve their responsiveness to inflammatory stimuli, the adult microglia cells were co-cultured with neurons dissected from hippocampi of rat embryos differentiated to mature neurons with >98% homogeneity (Gardoni et al., 2002). Bias of the co-culture was avoided by using a mix of male and female neurons.

Morphological analysis of microglia in culture (Benedusi et al., 2017) showed significant sex differences: 75% of male microglia had the globular morphology associated with the pro-inflammatory phenotype, and the remaining had the ramified branches connected with the surveilling status; in females, the percentage of activated microglia cells was much lower (50%) (Figure 2B). Consistent with this observation, qPCR on a subset of DEGs showed that the microglia grown in culture preserved, by and large, the expression pattern of the sex of origin (Figures 2C and 2D). Thus, microglia in culture appeared to maintain a gene expression characteristic of the sex of origin.

Female Microglia Retain Their Sex after Transplantation in the Male Brain

To better demonstrate that the transcriptome of adult microglia was sexually differentiated and independent of the *in vivo* hormonal environment, we investigated the gene expression profile of female microglia after transplantation into a male brain. In designing the transfer experiment, we anticipated several potential limitations, such as host versus graft reactions, microglia viability, and the ability to proliferate and migrate throughout the host brain. To facilitate the host brain repopulation by the transplanted microglia and limit adverse reactions, we first depleted the endogenous microglia. Previous reports had demonstrated that PLX3397, a small-molecule inhibitor of the CSF1 receptor (CSF1R) and related kinases, was able to promote selective microglia apoptosis (Elmore et al., 2014). This effect was transient, and microglia started to proliferate upon cessation of the treatment (Elmore et al., 2014). We administered PLX3397 via the transnasal (tsn) route to improve its permeation and diffusion throughout the brain parenchyma. Dose-response experiments allowed the identification of 100 μg/*die* as the minimum effective dose of PLX3397 necessary to deplete >90% of microglia after 7 days of treatment; no sign of toxicity was observed at higher dosages (data not shown). To be sure to maintain effective concentrations of PLX3397 in the brain, we treated the mice with 100 μg twice a day. The efficacy of the treatment was measured by the following: (1) counting the cells that were isolated from a single brain (Figure S2A); (2) measuring the whole brain content of the mRNA encoding the complement C1q subcomponent subunit A (C1qa), constitutively expressed in microglia (Fonseca et al., 2017) (Figure S2B); and (3) flow cytometry (Figure S2C). As reported previously in the literature (Elmore et al., 2014), at day 7, only a very small percentage (<8%) of the endogenous microglia was spared by the treatment; interruption of drug administration resulted in a rapid microglia proliferation starting 24 hr after the end of treatment,

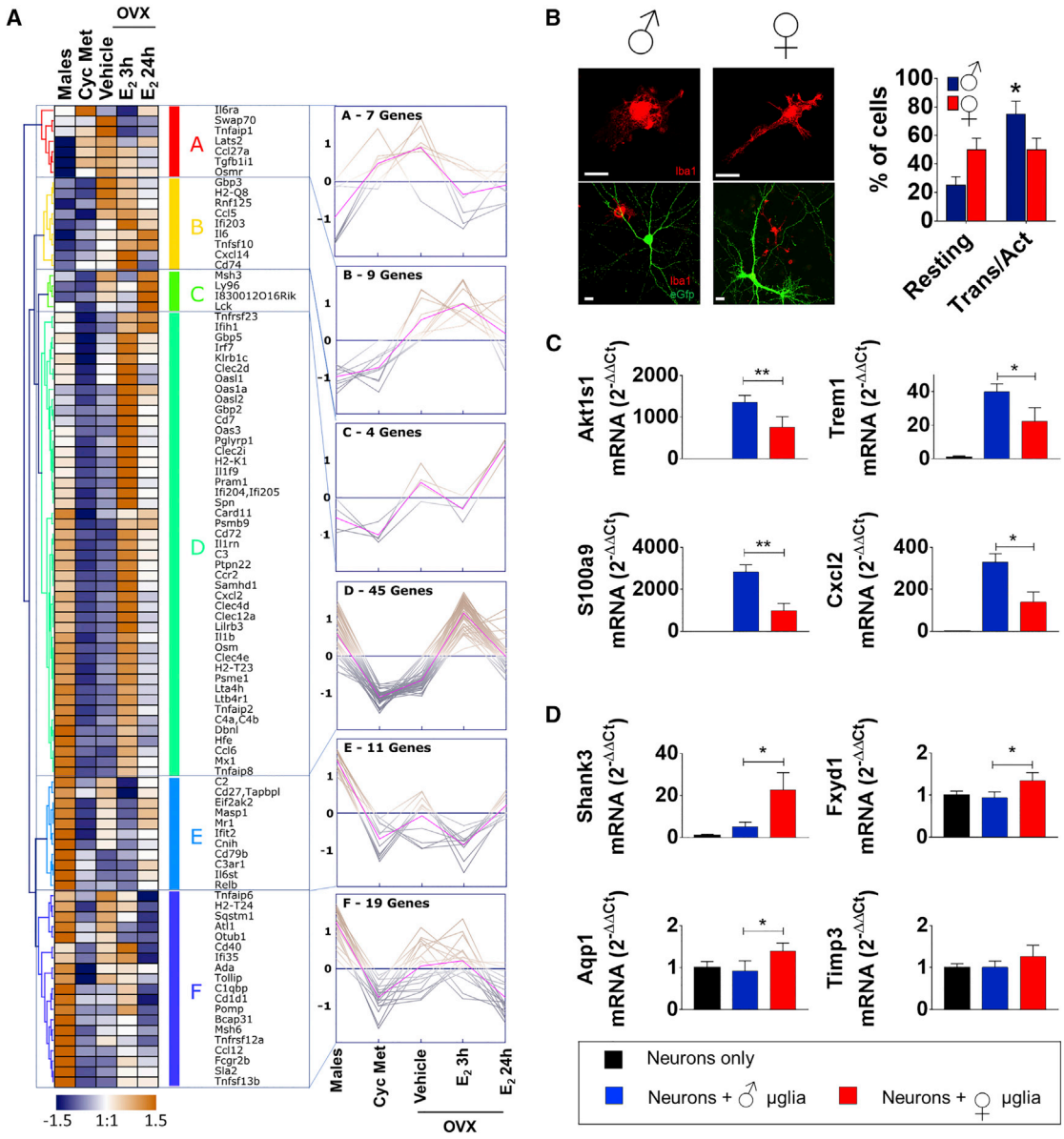

Figure 2. The Role of Estrogens in Preventing Microglia Inflammatory Phenotype

(A) Heatmap and hierarchical clustering of expression profiles for a subset of NF-κB-regulated genes measured in microglia, isolated from adult C57BL/6 mice: males, intact females (Cyc Met), and ovariectomized females treated with vehicle (OVX) or 17β-estradiol for 3 hr (OVX + E_2 3 hr) and 24 hr (OVX + E_2 24 hr). The group size was n = 2 samples per condition, each sample consisting of a pool of six brains. The results were log-transformed, normalized, and centered, and populations and genes were clustered by Pearson correlation. Data were obtained from two pools of six brains each. The right panel shows general expression plots for each cluster. The purple line represents the mean expression of the clustered genes.

(B) Immunocytochemistry of microglia stained with Iba1 antibody (red signal) showing different phenotypes in males or females. Upper panel: details of microglia (×100 magnification); lower panel: lower magnification images (×20) including neurons expressing EGFP (green). In the graph, each column corresponds to the percentage of cells showing either the resting or the activated phenotype. We blind-counted the cells present in 18 ×20 images (for about 200 cells/sex in total). The blind count was repeated by three different operators. *$p < 0.05$ by unpaired, two-tailed t test. Scale bar: 10 μm.

(C and D) qPCR analyses of genes showing higher expression in male (C) or female (D) microglia. Data are expressed as $2^{-\Delta\Delta Ct}$ using the 36B4 transcript as an internal reference standard. Each column represents the mean ± SEM of n = 6 plates measured in triplicate. *$p < 0.05$; **$p < 0.01$ by a one-way ANOVA and Tukey's method for multiple comparisons versus expression in neurons + male microglia (blue column).

and 5 days after ending PLX3397 administration, the brain content of microglia cells was back to normal (Figure S2A). Having established the procedure to eliminate the majority of the host microglia, we proceeded with the transplantation using microglia purified from female UBC-*luc2* (G4063), a transgenic mouse model where the expression of the luciferase reporter is

constitutive and not affected by sex and age (Rizzi et al., 2017). Prior to cell transplantation, we showed that in the isolated microglia, the light emission was directly proportional to the cell number (Figure S2D). For the cell transfer, we avoided brain injections and opted for the tsn route to preserve brain inflammatory homeostasis and blood-brain barrier integrity. A total number of 350,000–400,000 female bioluminescent microglia cells were tsn-transferred to the microglia-depleted male brains 24 hr after the interruption of PLX3397 treatment. The tsn administration enabled the distribution of cells throughout the forebrain and the caudal brain, including the brainstem and cerebellum (see Figure S2E and its legend). *Ex vivo* imaging (Stell et al., 2008) established that 3 days after the tsn administration, the bioluminescent exogenous microglia cells were located mainly in the cortex (Figure 3A). This was expected on the basis of the route of administration selected (Figure S2E). At day 5, the significant increase of bioluminescence indicated that the transplanted female microglia were actively proliferating; furthermore, these cells had spread in most brain areas including the cortex, hippocampus, caudate and putamen, thalamus, hypothalamus, mid-brain, and pons (Figure S2F). The presence in the recipient male brain of an mRNA that is exclusively expressed in females, the X-inactive specific transcript (*Xist*), demonstrated that the transfer experiment had been successful (Figure 3C). In addition, the exogenous microglia were alive and transcriptionally active because the amount of *Xist* mRNA detectable 3 days after the transfer was increased at day 5 (Figure 3C). At day 5, the ratio of *Xist* to *C1qa* mRNAs indicated that the transplanted female cells were approximately 19% of the total host brain microglia (Figure 3C); this amount was confirmed by flow cytometry of CX3CR1-GFP male microglia transplanted in wild-type (males or females) (Figure S2G); the same experiment allowed to demonstrate that the transplanted cells maintained the expression of microglia-specific biomarkers (Tmem119) (Bennett et al., 2016) (Figure S2H). Further experiments with female or male microglia transplanted into male recipients (F/M or M/M, respectively) established that the sex of origin did not influence the ability of these cells to proliferate; indeed, Figure 3D shows that the expressions of selected genes (*C1qa* marker of total microglia content, *Ki67* associated with cell proliferation, and *Cdk3* expressed during G0–G1 and G1–S cell-cycle transitions) was the same in male or female transplanted cells. To investigate the extent to which the transplanted microglia preserved their sex-specific identity, we transplanted fluorescent microglia (from male or female CX3CR1-GFP mice) in WT males and analyzed the expression of selected genes in the fluorescent cells isolated by FACS. Male fluorescent cells transplanted in males (M/M) maintained the male-specific (M) profile of expression (relatively high *Akt1s1*, *Trem1*, *S100a9*, and *Cxcl2* and low *Shank3*, *Fxyd1*, *Aqp1*, and *Timp3*); female cells transplanted in males (F/M) were able to keep a profile of expression superimposable with that of the control females (F) (Figures 3E and 3F).

The combination of all the experiments conducted highlighted the possibility of a genomic and/or epigenetic component that sexually differentiates microglia gene expression. It is known that the perinatal androgen surge from male testis and the subsequent local aromatization of testosterone to estradiol is crucial for the permanent modification of neuronal functions characteristic of brain masculinization (Arnold and Gorski, 1984; McCarthy and Nugent, 2015; Villa et al., 2016). In line with these reports, imaging experiments on ERE-Luc mice showed that perinatal activation of ERα is restricted to males (Figures S3A and S3B). To directly show that in addition to neurons the perinatal exposure to estrogens could affect microglia gene expression permanently, we followed a classical protocol of brain masculinization by treating male and female pups with E_2 benzoate at days P2, P5, and P8 (McCarthy, 2008; Wu et al., 2009). The masculinized females were unable to cycle at 6–8 weeks of age, demonstrating the efficacy of the protocol. The extent to which the treatment had affected microglia gene expression was assessed by qPCR of the four DEGs previously identified as more expressed in males. Figure 3G shows that in the microglia extracted from the masculinized brains, the expression of *Akts*, *Trem1*, and *CxCl2* was not significantly different than in males; *S100a9* was not affected by the brain masculinization.

Protective Action of Female Microglia in Ischemia

We next asked whether microglia sex-specific gene expression had any functional relevance. Several authors demonstrated that in the case of forebrain or focal ischemia, young adult female rodents sustain smaller injury than males, and females have lower mortality than males (Murphy et al., 2004; Spychala et al., 2017). The course of microglia activation after cerebral ischemia has been largely described, and it is well known that microglia proliferation at the infarct site limits the ischemic damage possibly because microglia generate neurotrophic factors that are beneficial for neuronal plasticity (Lalancette-Hébert et al., 2007). Considering this fact, and based on the results obtained with our RNA-seq analyses that unstimulated female microglia have a higher propensity than male microglia to express genes involved in cell plasticity, the control of the inflammatory response, and repair mechanisms, we questioned whether transferring female microglia into male brains would have restricted the brain damage consequent to ischemia. First, we subjected adult WT male (n = 6) and female (n = 6) mice to permanent focal cerebral ischemia (permanent middle cerebral artery occlusion [pMCAO]) (Gelosa et al., 2014), and we carried out diffusion-weighted imaging (DWI) at 2, 24, and 48 hr after the ischemic insult. In DWI, the ischemic lesion appears hypointense, consistent with a decrease in the apparent diffusion coefficient of water (ADC), which is a weighted average between the intracellular (assumed to be lower) and extracellular diffusion coefficients (assumed to be higher). The decrease in ADC reflects the changes in the ratio of intracellular and extracellular volume, because ischemia-induced energy impairment and membrane pump failure allow the osmotic drainage of water from extracellular to intracellular spaces that leads to cytotoxic edema (van Gelderen et al., 1994). The results obtained in control animals (Figure S4A) showed that in males, the damaged area at 24 and 48 hr was larger than in females, which is in line with previous reports (Spychala et al., 2017). Next, we transplanted 16 adult male mice with microglia purified either from male (n = 8 M/M) or female mice (n = 8 F/M). Figure 4A shows the DWI of the transplanted mice at 2, 24, and 48 hr after ischemia. At 2 hr

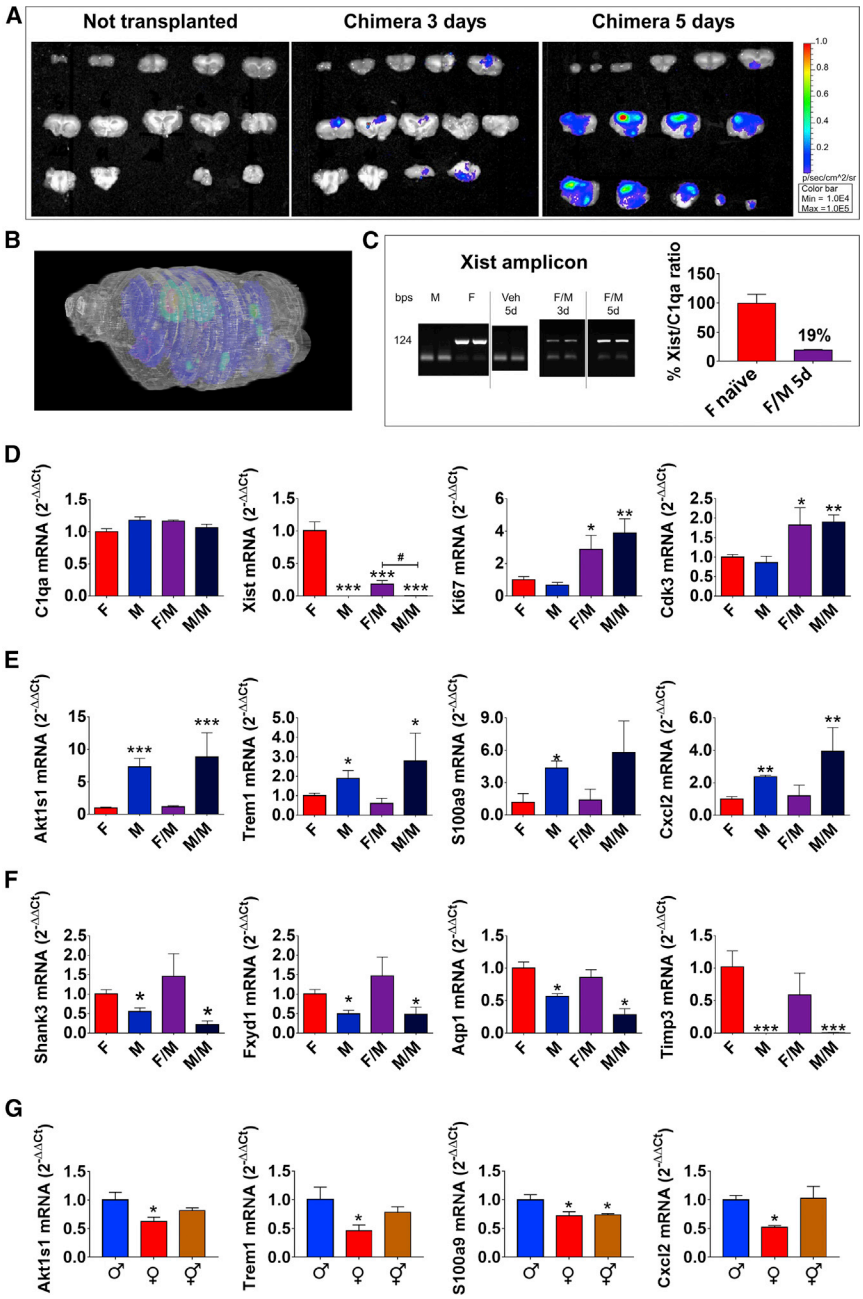

Figure 3. Female Microglia Maintain Their Characteristic Gene Expression When Transplanted in Male Brain

(A) Bioluminescence-based optical imaging of brain slices of WT male mice before (left panel) and after (3 days, central panel; 5 days, right panel) transnasal administration of 400,000 bioluminescent microglial cells isolated from female G4063 mice; pseudocolors represent the intensity of light emission (p/s/cm^2/sr). The images are representative of three independent measures on n = 3 individual animals/group.

(B) Three-dimensional representation of the distribution of bioluminescent signals in WT mouse brain, 5 days after transnasal administration of bioluminescent microglial cells isolated from G4063 mice. Pseudocolors represent the intensity of light emission (p/s/cm^2/sr), according to the color bar reported in (A).

(C) RT-PCR analysis was performed using primers for Xist mRNA (amplicon: 124 bp) on microglia RNA isolated from naive male (M) or female (F) mice, vehicle-treated male mice (Veh, 5 days [5d]) or after transnasal administration of 400,000 microglial cells isolated from female C57BL/6 mice (F/M 3d: microglia isolated 3 days after transnasal administration; F/M 5d: microglia isolated 5 days after transnasal administration). Bars represent the percentage ratio of Xist and C1qa mRNA accumulation in naive female microglia (two independent measures, n = 3) or in microglia derived from males, 5 days after transnasal administration of 400,000 microglial cells isolated from female C57BL/6 mice (5d: microglia isolated 5 days after transnasal administration, two independent measures, n = 3). Data are normalized to naive female mice.

(D) qPCR analyses of C1qa, Xist, Ki67, and Cdk3 mRNA accumulation in microglia isolated from naive female (F) or male (M) mice or 5 days after transnasal administration of 400,000 microglial cells isolated from female (F/M) or male (M/M) C57BL/6 mice. Data are expressed as $2^{-\Delta\Delta Ct}$ using the 36B4 transcript as an internal reference standard. Columns represent the mean ± SEM of n = 6 animals measured in triplicates. *p < 0.05; **p < 0.01; ***p < 0.001 by a one-way ANOVA and Tukey's method for multiple comparisons versus (F). $^{\#}$p < 0.05 by a two-way ANOVA and Tukey's method for multiple comparisons.

(E) qPCR analyses of Shank3, Fxyd1, Aqp1, and Timp3 mRNA accumulation in microglia isolated from naive female (F) or male (M) mice or fluorescence-sorted 5 days after transnasal administration of 400,000 microglial cells isolated from female (F/M) or male (M/M) CX3CR1-GFP mice. Data are expressed as $2^{-\Delta\Delta Ct}$ using the 36B4 transcript as an internal reference standard. Columns represent the mean ± SEM of n = 6 animals measured in triplicates. *p < 0.05; **p < 0.01; ***p < 0.001 by a one-way ANOVA and Tukey's method for multiple comparisons versus (F). $^{\#}$p < 0.05 by a two-way ANOVA and Tukey's method for multiple comparisons.

(F) qPCR analyses of Akt1s1, Trem1, S100a9, and Cxcl2 mRNA accumulation in microglia isolated from naive female (F) or male (M) mice or fluorescence-sorted 5 days after transnasal administration of 400,000 microglial cells isolated from female (F/M) or male (M/M) CX3CR1-GFP mice. Data are expressed as $2^{-\Delta\Delta Ct}$ using the 36B4 transcript as an internal reference standard. Columns represent the mean ± SEM of n = 6 animals measured in triplicates. *p < 0.05; **p < 0.01; ***p < 0.001 by a one-way ANOVA and Tukey's method for multiple comparisons versus microglia isolated from naive female mice. $^{\#}$p < 0.05; $^{\#\#\#}$p < 0.001 by a two-way ANOVA and Tukey's method for multiple comparisons.

(G) qPCR analyses of Akt1s1, Trem1, S100a9, and Cxcl2 mRNA accumulation in microglia isolated from naive male (♂), female (♀), or masculinized female (⚥) C57BL/6 mice. Data are expressed as $2^{-\Delta\Delta Ct}$ using the 36B4 transcript as an internal reference standard. Columns represent the mean ± SEM of n = 6 animals measured in triplicates. *p < 0.05 by a one-way ANOVA and Tukey's method for multiple comparisons versus ♂.

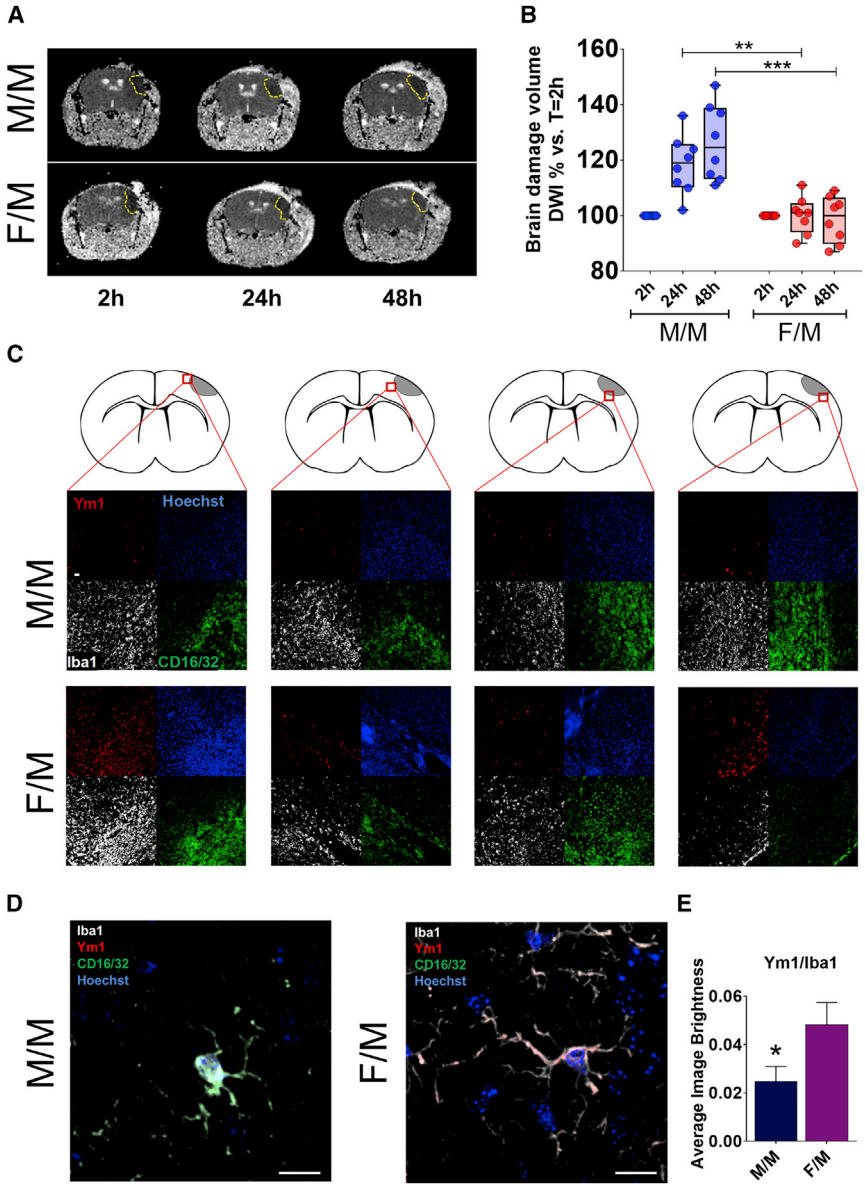

Figure 4. Sex of Microglia Influence the Progression of Ischemic Stroke

(A) Time-dependent evolution of infarct volume in permanent middle cerebral artery occlusion (pMCAO) mice. Diffusion-weighted imaging (DWI) representative of male mice transnasally administered with male (M/M) or female (F/M) microglia, taken at 2, 24, and 48 hr after pMCAO. The ischemic lesion is detectable as a hypointense area in the right cerebral hemisphere (delineated by the yellow dotted line). The image is representative of n = 8 animals.

(B) Scatterplot showing the quantitative analysis of the brain damage volume determined by DWI measurements and expressed as percent change relative to the initial 2 hr value set to 100%. Solid lines represent mean ± SEM for M/M (n = 8) and F/M mice (n = 8). **p < 0.01; ***p < 0.001 by two-way ANOVA and Sidak's method for multiple comparisons.

(C) Representative, low-magnification (×20) immunofluorescence analysis of coronal sections of brains excised from adult mice that had undergone pMCAO, stained for Iba1 (white), CD16/32 (green), Ym1 (red), and Hoechst 33258 (blue). M/M: male recipient transplanted with male microglia; F/M: male recipient transplanted with female microglia. Images are representative of n = 3 mice per experimental group and show the fluorescence images acquired in the areas indicated by red squares in the upper schematics. Scale bar: 10 μm.

(D) Representative high-magnification (×100) confocal z stack projections of cells stained for Iba1 (white), CD16/32 (green), Ym1 (red), and Hoechst 33258 (blue) in mice that had undergone pMCAO. The pictures show the colocalization of pro- (CD16/32) and anti-inflammatory markers with Iba1-stained microglia. M/M: male recipient transplanted with male microglia; F/M: male recipient transplanted with female microglia. Images are representative of n = 3 mice per experimental group. Scale bar: 10 μm.

(E) Graph columns show the mean ± SEM of fluorescence brightness for Ym1 (red channel) in Iba1-positive cells, measured in a double-blind manner. *p < 0.05 by unpaired, two-tailed t test.

after the infarct, the sex of origin of the transplanted microglia did not influence the volume of the damage (Figure S4B). This was expected because in our experience, changes in the damage size are not detectable at early phase after ischemia (Gelosa et al., 2014). In the M/M group, the progression of the damage was significantly higher (+26% after 48 hr) than in the F/M group (Figure 4B), thus pointing to a protective action of the female microglia. Male microglia into female brain (n = 8) did not provide as clear and significant results (Figure S4C).

To determine the ability of exogenous microglia to migrate to the infarct site, we subjected mice transplanted with bioluminescent G4063 microglia to pMCAO. Bioluminescence imaging revealed that after pMCAO, a large amount of the bioluminescent, exogenous microglia accumulated in the vicinity of the infarct site (Figure S4D). The phenotype of microglia at the lesion site was investigated by immunostaining of the pMCAO lesioned brain. We used Ab against Ym1 as a marker for microglia anti-inflammatory activation and against CD16/32 as a marker for pro-inflammatory activation (Figure 4C). Low-magnification confocal imaging of the fields of view surrounding the ischemic lesion revealed that Ym1 immunoreactivity was higher in brain samples obtained from the F/M animals. At higher magnification (×100), the immunofluorescence showed that both CD16/32 and Ym1 co-localized with Iba1 immunoreactivity (Figure 4D). Semiquantitative, double-blind analyses of the average fluorescence brightness in Iba1-positive cells surrounding the ischemic lesion showed Ym1 immunoreactivity significantly higher (+92%) in F/M versus M/M (Figure 4E). CD16/32 staining was comparable in both experimental groups (Figure S4E).

DISCUSSION

The present study shows that microglia cells are sexually differentiated, as indicated by the sex-specific expression of a significant number of genes. Microglia cells maintain sex-specific expression independently by the circulating sex steroids, which was demonstrated by putting adult microglia in culture or by their transplant in the opposite sex. In addition, ovariectomy did not show very significant changes in microglia gene expression. The mechanism involved in microglia sexual differentiation remains to be determined. The fact that neonatal treatment of female brain with estrogens (using a protocol known to induce brain defemination) altered the expression of selected genes may suggest that similar to what was reported for neurons, the sex of microglia is determined at birth. Microglia are an autonomous self-proliferating population of cells that migrate from the yolk sac prior to hematopoiesis. Following brain colonization, these cells differentiate into microglia, and the formation of the blood-brain barrier prevents the infiltration of peripheral cells, at least under healthy conditions. Therefore, the masculinizing surge of testosterone might induce the differentiation of this cell population, because neonatal microglia express the estrogen receptor alpha (Crain et al., 2013; Sierra et al., 2008). Other authors studying microglia in embryos, neonates, and adult mice showed that there are precise temporal phases that characterize microglia development (Matcovitch-Natan et al., 2016), and that the immune reactivity of these cells is sexually differentiated very early in development (Hanamsagar et al., 2017). In addition, during the first week postpartum in mice, there are sexual differences in the morphology and the number of these cells (Lenz et al., 2013), and microglia have an inflammatory morphology that converts to a largely ramified state occurring by the third week after birth when male defemination is completed. These observations have suggested that microglia in the neonatal brain are involved in more than a response to brain injury or inflammation; that is, microglia actively participate in the formation of specific brain circuitries by regulating a variety of developmental processes and physiological functions including synapse elimination, spinogenesis, spine elimination, and synaptic physiology (Tremblay et al., 2011).

Our study suggests that the local neonatal synthesis of estrogen associated with the androgen surge from the male testis may not be a cause of transient activation of microglia but might have permanent (organizational) effects on these cells by inducing a sexual phenotype that is maintained in the adult animals. This would explain why male or female microglia have the tendency to maintain the same gene expression when transplanted in the opposite sex. Indeed, analogous to what occurs in neurons where their sensitivity and ability to respond to specific hormonal and environmental stimuli (activational effects) is permanently affected by the neonatal estrogen priming, our data suggest that in male microglia, the estrogen priming changes their immune capacity by enhancing their ability to react to inflammatory stimuli. These data are in agreement with a very recent study aimed at comparing the male and female microglia transcriptome in relation with the stage of development (Hanamsagar et al., 2017).

We do not know what the teleological meaning of this sexual differentiation is; certainly, our studies show that this biological event has functional repercussions on the damage caused from acute cerebral ischemia (MCAO) (Figure 4). It is well known that the damage induced by MCAO is significantly higher in males than in females, and several studies have debated whether this is due to a lower susceptibility of female neurons to ischemia or to differences in the evolution of the neuroinflammatory response (Murphy et al., 2004). The findings reported here that female microglia are better apt than male microglia to reduce the ischemic damage also when transplanted in males highlight an intrinsic sex-specific microglia phenotype that might be independent from the hormonal environment. This is in line with the observation that in humans, males have a higher incidence of stroke and poorer outcomes afterward (Golomb et al., 2009). However, we cannot definitively conclude that estrogens do not influence microglia activity, because aromatase is expressed in the male brain and may convert locally the circulating testosterone into estradiol (McCullough et al., 2003).

Our results point to microglia as major actors in the evolution of the ischemic insult; this is in accordance with prior literature, as our observations were conducted at 24 and 48 hr after ischemia. Morphological, immunohistochemical, MRI-based, and pharmacological studies have shown that in the first 72 hr after ischemia, the CNS resident microglia control the course of inflammation, generating anti-inflammatory or repair molecules in the insult area (Gelderblom et al., 2009; Rupalla et al., 1998). Additionally, microglia participate in attracting peripheral immune cells that populate the damaged area at later times (Gelderblom et al., 2009). At this point, it is possible that in females, the presence of circulating estrogens limits the damage caused by an excessive inflammatory response, because female monocytic cells were shown to better transit toward the anti-inflammatory phenotype (Villa et al., 2015) and were likely able to confine the tissue damage induced by the hypoxic stimulus, possibly by virtue of the limited expression of genes encoding inflammatory proteins. Interestingly, when we transplanted male microglia into female brains, we did not observe an increase in the ischemic area with time. This might be because the female resident microglia buffered the effects of the grafted cells.

Neuropsychiatric or neurological diseases may manifest in a large percentage of the population (approximately 25% of individuals suffer from brain disorders in their lifespan) with a pattern of susceptibility that is associated with sex. Females are more affected by diseases that occur during adulthood, whereas males are particularly vulnerable to life-long illnesses of neurodevelopmental origin. Considering the number of studies underscoring the relevance of inflammation in brain disturbances, the finding of a sex difference in male and female susceptibility to neuroinflammation provides a basis for a sex-related approach to therapy that must be based on a better understanding of the relationships among the endocrine, immune, and nervous systems in young and adult individuals.

EXPERIMENTAL PROCEDURES

Animals

Animal studies were carried out at the Department of Pharmacological and Biomolecular Sciences. All animal experimentation was carried out in accordance with the ARRIVE and European Guidelines for Animal Care. All animal experiments were approved by the Italian Ministry of Research and University (permission numbers: 12-12-30012012, 547/2015, 479/2015) and controlled by a departmental panel of experts.

C57BL/6 and CX3CR1-GFP mice at 3 months of age were supplied by Charles River (Charles River Laboratories, Calco, Italy). Both male and female mice were used throughout experiments as described earlier. Animals were allowed access to food and water *ad libitum* and kept in temperature-controlled facilities on a 12-hr light and dark cycle. More details are available in the Supplemental Experimental Procedures.

Pharmacological Manipulations

E_2 (Sigma-Aldrich, Italy) was administered by a 100 μL s.c. injection of 5 μg/kg E_2 (which results in circulating E_2 levels comparable with those at proestrus [Ciana et al., 2003]) dissolved in corn oil by overnight (o/n) stirring in the dark at room temperature; control animals received corn oil injection alone. E_2 benzoate was administered by a s.c. injection of 5 μg in 50 μL of corn oil; control animals received corn oil alone.

Microglia Sorting

Isolation of microglia from the whole brains of adult mice was performed as described in Pepe et al. (2014). More details are available in the Supplemental Experimental Procedures.

PLX3397 Administration

8.3 mg of PLX3397 was dissolved in 1 mL of 5% DMSO + 45% polyethylene glycol 300 (PEG300) + ddH_2O (double-distilled water) solution. Prior to tsn administration, animals were anesthetized with s.c. injection of 50 μL solution of ketamine (93.6 mg/kg, Ketavet 100; Intervet, Milan, Italy) and xylazine (7.2 mg/kg, Rompun; Bayer, Milan, Italy). More details are available in the Supplemental Experimental Procedures.

Cell Cultures

Primary neuronal cultures were obtained from the hippocampi of 18-day-old fetal Sprague Dawley rats of both sexes (Charles River Italia). Neurons were transfected at 7 days *in vitro* (*DIV7*) using the calcium-phosphate method with 2 μg of EGFP plasmid. At *DIV10* microglia were isolated from the brain of adult mice and seeded over rat neurons with a microglia:neuron ratio of 1:10. At *DIV14*, cells were either processed for immunocytochemistry or resuspended in TRIzol reagent (Invitrogen, Milan, Italy) and processed for RNA preparation.

Morphological Analysis of Iba1-Stained Microglia

Three images of six slides per experimental condition were taken. The size of the fields analyzed was 173 μm × 218 μm. Morphological analyses were performed in a double-blind manner as previously described (Benedusi et al., 2017). ImageJ software was used to measure immunoreactivity through a threshold method, and the number of positive pixels and the extension of area of interest were used to determine the fractional area covered by the specific signal.

Brain Masculinization

Pregnant C57BL/6 mice were individually housed after pups' birth. All pups within a litter were subcutaneously injected with vehicle (50 μL corn oil) or treatment (5 μg E_2 benzoate in 50 μL corn oil) (Wu et al., 2009) at post-natal day 2 (P2), P5, and P8. At P21, females and males were housed in separate cages. At 10–14 weeks of age, vaginal smears were carried out to study the ability of the females to cycle.

MRI Analysis

Brain infarct size was visualized by DWI at 2, 24, and 48 hr after MCAO using a 4.7 T, vertical super-wide bore magnet of a Bruker Avance II spectrometer with microimaging accessory. More details are available in the Supplemental Experimental Procedures.

Statistical Analyses

Statistical analysis of RNA-seq data were carried out using the CuffDiff (Trapnell et al., 2012) software. A t test was used to calculate the p value for differential expression. A threshold of 0.01 was applied to FDR-adjusted p values (q values) in order to select the DEGs to use in downstream analyses. Cluster analyses were performed with the Genesis software tool (https://genome.tugraz.at/genesisclient/genesisclient_description.shtml) to log-transform, normalize, and center gene expressions, and populations and genes were clustered by Pearson correlation. Overrepresentation analysis (ORA) on DEG lists was performed using Enrichr for enrichment analysis. The mouse genome was used as background list. Biological processes, molecular functions, and KEGG pathways were investigated focusing on enriched terms with a Benjamini-adjusted p value less than 0.05.

Statistical significance of the other reported data were calculated using Prism 7 software (GraphPad); unless otherwise indicated in the figure legend, one-way ANOVA for single-treatment comparisons or two-way ANOVA for multiple treatment comparisons was applied. A p value less than 0.05 was considered as statistically significant.

DATA AND SOFTWARE AVAILABILITY

The accession number for the RNA-seq data reported in this paper is NCBI Sequence Read Archive: SRP104620.

SUPPLEMENTAL INFORMATION

Supplemental Information includes Supplemental Experimental Procedures and four figures and can be found with this article online at https://doi.org/10.1016/j.celrep.2018.05.048.

ACKNOWLEDGMENTS

We thank Monica Rebecchi and Clara Meda for their continuous assistance throughout the study, Nicolò Panini for technical assistance, and Tiziana Borsello for the critical reading of the manuscript. The authors are supported by European Union grant ERC-2012-ADG322977-Ways and the Seventh Framework Programme (FP7/2007–2013) under grant agreement no. 278850 (INMiND).

AUTHOR CONTRIBUTIONS

Conceptualization, A.M. and A.V.; Methodology, A.M., A.V., and N.R.; Investigation, A.V., P.G., M.C., N.R., E.M., F.L., G.P., and L.C.; Writing – Original Draft, A.M. and A.V.; Writing – Review & Editing, A.V., A.M., L.S., E.M., and P.G.; Funding Acquisition, A.M.; Resources, A.M. and L.S.; Supervision, A.M., L.S., and E.V.

DECLARATION OF INTERESTS

The authors declare no competing interests.

Received: September 27, 2017
Revised: April 6, 2018
Accepted: May 14, 2018
Published June 19, 2018

REFERENCES

Arnold, A.P., and Gorski, R.A. (1984). Gonadal steroid induction of structural sex differences in the central nervous system. Annu. Rev. Neurosci. *7*, 413–442.

Balli, D., Ren, X., Chou, F.S., Cross, E., Zhang, Y., Kalinichenko, V.V., and Kalin, T.V. (2012). Foxm1 transcription factor is required for macrophage migration during lung inflammation and tumor formation. Oncogene *31*, 3875–3888.

Benedusi, V., Della Torre, S., Mitro, N., Caruso, D., Oberto, A., Tronel, C., Meda, C., and Maggi, A. (2017). Liver ERα regulates AgRP neuronal activity in the arcuate nucleus of female mice. Sci. Rep. *7*, 1194.

Bennett, M.L., Bennett, F.C., Liddelow, S.A., Ajami, B., Zamanian, J.L., Fernhoff, N.B., Mulinyawe, S.B., Bohlen, C.J., Adil, A., Tucker, A., et al. (2016). New tools for studying microglia in the mouse and human CNS. Proc. Natl. Acad. Sci. USA *113*, E1738–E1746.

Ciana, P., Raviscioni, M., Mussi, P., Vegeto, E., Que, I., Parker, M.G., Lowik, C., and Maggi, A. (2003). In vivo imaging of transcriptionally active estrogen receptors. Nat. Med. *9*, 82–86.

Crain, J.M., Nikodemova, M., and Watters, J.J. (2013). Microglia express distinct M1 and M2 phenotypic markers in the postnatal and adult central nervous system in male and female mice. J. Neurosci. Res. *91*, 1143–1151.

Duan, Z., Ma, C., Han, Y., Li, Y., and Zhou, H. (2013). Nanog attenuates lipopolysaccharide-induced inflammatory responses by blocking nuclear factor-κB transcriptional activity in BV-2 cells. Neuroreport *24*, 718–723.

El Wakil, A., Francius, C., Wolff, A., Pleau-Varet, J., and Nardelli, J. (2006). The GATA2 transcription factor negatively regulates the proliferation of neuronal progenitors. Development *133*, 2155–2165.

Elmore, M.R., Najafi, A.R., Koike, M.A., Dagher, N.N., Spangenberg, E.E., Rice, R.A., Kitazawa, M., Matusow, B., Nguyen, H., West, B.L., and Green, K.N. (2014). Colony-stimulating factor 1 receptor signaling is necessary for microglia viability, unmasking a microglia progenitor cell in the adult brain. Neuron *82*, 380–397.

Fonseca, M.I., Chu, S.H., Hernandez, M.X., Fang, M.J., Modarresi, L., Selvan, P., MacGregor, G.R., and Tenner, A.J. (2017). Cell-specific deletion of C1qa identifies microglia as the dominant source of C1q in mouse brain. J. Neuroinflammation *14*, 48.

Gardoni, F., Bellone, C., Viviani, B., Marinovich, M., Meli, E., Pellegrini-Giampietro, D.E., Cattabeni, F., and Di Luca, M. (2002). Lack of PSD-95 drives hippocampal neuronal cell death through activation of an alpha CaMKII transduction pathway. Eur. J. Neurosci. *16*, 777–786.

Gelderblom, M., Leypoldt, F., Steinbach, K., Behrens, D., Choe, C.U., Siler, D.A., Arumugam, T.V., Orthey, E., Gerloff, C., Tolosa, E., and Magnus, T. (2009). Temporal and spatial dynamics of cerebral immune cell accumulation in stroke. Stroke *40*, 1849–1857.

Gelosa, P., Lecca, D., Fumagalli, M., Wypych, D., Pignieri, A., Cimino, M., Verderio, C., Enerbäck, M., Nikookhesal, E., Tremoli, E., et al. (2014). Microglia is a key player in the reduction of stroke damage promoted by the new antithrombotic agent ticagrelor. J. Cereb. Blood Flow Metab. *34*, 979–988.

Golomb, M.R., Fullerton, H.J., Nowak-Gottl, U., and Deveber, G.; International Pediatric Stroke Study Group (2009). Male predominance in childhood ischemic stroke: findings from the international pediatric stroke study. Stroke *40*, 52–57.

Hanamsagar, R., Alter, M.D., Block, C.S., Sullivan, H., Bolton, J.L., and Bilbo, S.D. (2017). Generation of a microglial developmental index in mice and in humans reveals a sex difference in maturation and immune reactivity. Glia *65*, 1504–1520.

Hooper, L.V., Littman, D.R., and Macpherson, A.J. (2012). Interactions between the microbiota and the immune system. Science *336*, 1268–1273.

Hu, X., Leak, R.K., Shi, Y., Suenaga, J., Gao, Y., Zheng, P., and Chen, J. (2015). Microglial and macrophage polarization—new prospects for brain repair. Nat. Rev. Neurol. *11*, 56–64.

Kettenmann, H., Kirchhoff, F., and Verkhratsky, A. (2013). Microglia: new roles for the synaptic stripper. Neuron *77*, 10–18.

Kierdorf, K., and Prinz, M. (2013). Factors regulating microglia activation. Front. Cell. Neurosci. *7*, 44.

Kierdorf, K., and Prinz, M. (2017). Microglia in steady state. J. Clin. Invest. *127*, 3201–3209.

Kuleshov, M.V., Jones, M.R., Rouillard, A.D., Fernandez, N.F., Duan, Q., Wang, Z., Koplev, S., Jenkins, S.L., Jagodnik, K.M., Lachmann, A., et al. (2016). Enrichr: a comprehensive gene set enrichment analysis web server 2016 update. Nucleic Acids Res. *44* (*W1*), W90–W97.

Lalancette-Hébert, M., Gowing, G., Simard, A., Weng, Y.C., and Kriz, J. (2007). Selective ablation of proliferating microglial cells exacerbates ischemic injury in the brain. J. Neurosci. *27*, 2596–2605.

Lenz, K.M., Nugent, B.M., Haliyur, R., and McCarthy, M.M. (2013). Microglia are essential to masculinization of brain and behavior. J. Neurosci. *33*, 2761–2772.

MacLusky, N.J., and Naftolin, F. (1981). Sexual differentiation of the central nervous system. Science *211*, 1294–1302.

Matcovitch-Natan, O., Winter, D.R., Giladi, A., Vargas Aguilar, S., Spinrad, A., Sarrazin, S., Ben-Yehuda, H., David, E., Zelada González, F., Perrin, P., et al. (2016). Microglia development follows a stepwise program to regulate brain homeostasis. Science *353*, aad8670.

McCarthy, M.M. (2008). Estradiol and the developing brain. Physiol. Rev. *88*, 91–124.

McCarthy, M.M., and Nugent, B.M. (2015). At the frontier of epigenetics of brain sex differences. Front. Behav. Neurosci. *9*, 221.

McCullough, L.D., Blizzard, K., Simpson, E.R., Oz, O.K., and Hurn, P.D. (2003). Aromatase cytochrome P450 and extragonadal estrogen play a role in ischemic neuroprotection. J. Neurosci. *23*, 8701–8705.

Miao, Q., Ku, A.T., Nishino, Y., Howard, J.M., Rao, A.S., Shaver, T.M., Garcia, G.E., Le, D.N., Karlin, K.L., Westbrook, T.F., et al. (2014). Tcf3 promotes cell migration and wound repair through regulation of lipocalin 2. Nat. Commun. *5*, 4088.

Murphy, S.J., McCullough, L.D., and Smith, J.M. (2004). Stroke in the female: role of biological sex and estrogen. ILAR J. *45*, 147–159.

Neumann, H., Kotter, M.R., and Franklin, R.J. (2009). Debris clearance by microglia: an essential link between degeneration and regeneration. Brain *132*, 288–295.

Olsson, A., Venkatasubramanian, M., Chaudhri, V.K., Aronow, B.J., Salomonis, N., Singh, H., and Grimes, H.L. (2016). Single-cell analysis of mixed-lineage states leading to a binary cell fate choice. Nature *537*, 698–702.

Pepe, G., Calderazzi, G., De Maglie, M., Villa, A.M., and Vegeto, E. (2014). Heterogeneous induction of microglia M2a phenotype by central administration of interleukin-4. J. Neuroinflammation *11*, 211.

Prinz, M., and Priller, J. (2014). Microglia and brain macrophages in the molecular age: from origin to neuropsychiatric disease. Nat. Rev. Neurosci. *15*, 300–312.

Rizzi, N., Rebecchi, M., Levandis, G., Ciana, P., and Maggi, A. (2017). Identification of novel loci for the generation of reporter mice. Nucleic Acids Res. *45*, e37.

Rupalla, K., Allegrini, P.R., Sauer, D., and Wiessner, C. (1998). Time course of microglia activation and apoptosis in various brain regions after permanent focal cerebral ischemia in mice. Acta Neuropathol. *96*, 172–178.

Salter, M.W., and Stevens, B. (2017). Microglia emerge as central players in brain disease. Nat. Med. *23*, 1018–1027.

Schafer, D.P., Lehrman, E.K., and Stevens, B. (2013). The "quad-partite" synapse: microglia-synapse interactions in the developing and mature CNS. Glia *61*, 24–36.

Sierra, A., Gottfried-Blackmore, A., Milner, T.A., McEwen, B.S., and Bulloch, K. (2008). Steroid hormone receptor expression and function in microglia. Glia *56*, 659–674.

Spychala, M.S., Honarpisheh, P., and McCullough, L.D. (2017). Sex differences in neuroinflammation and neuroprotection in ischemic stroke. J. Neurosci. Res. *95*, 462–471.

Stell, A., Belcredito, S., Ciana, P., and Maggi, A. (2008). Molecular imaging provides novel insights on estrogen receptor activity in mouse brain. Mol. Imaging *7*, 283–292.

Trapnell, C., Roberts, A., Goff, L., Pertea, G., Kim, D., Kelley, D.R., Pimentel, H., Salzberg, S.L., Rinn, J.L., and Pachter, L. (2012). Differential gene and transcript expression analysis of RNA-seq experiments with TopHat and Cufflinks. Nat. Protoc. *7*, 562–578.

Tremblay, M.E., Stevens, B., Sierra, A., Wake, H., Bessis, A., and Nimmerjahn, A. (2011). The role of microglia in the healthy brain. J. Neurosci. *31*, 16064–16069.

van Gelderen, P., de Vleeschouwer, M.H., DesPres, D., Pekar, J., van Zijl, P.C., and Moonen, C.T. (1994). Water diffusion and acute stroke. Magn. Reson. Med. *31*, 154–163.

Vegeto, E., Bonincontro, C., Pollio, G., Sala, A., Viappiani, S., Nardi, F., Brusadelli, A., Viviani, B., Ciana, P., and Maggi, A. (2001). Estrogen prevents the lipopolysaccharide-induced inflammatory response in microglia. J. Neurosci. *21*, 1809–1818.

Vegeto, E., Ciana, P., and Maggi, A. (2002). Estrogen and inflammation: hormone generous action spreads to the brain. Mol. Psychiatry *7*, 236–238.

Villa, A., Rizzi, N., Vegeto, E., Ciana, P., and Maggi, A. (2015). Estrogen accelerates the resolution of inflammation in macrophagic cells. Sci. Rep. *5*, 15224.

Villa, A., Vegeto, E., Poletti, A., and Maggi, A. (2016). Estrogens, neuroinflammation, and neurodegeneration. Endocr. Rev. *37*, 372–402.

Wu, M.V., Manoli, D.S., Fraser, E.J., Coats, J.K., Tollkuhn, J., Honda, S., Harada, N., and Shah, N.M. (2009). Estrogen masculinizes neural pathways and sex-specific behaviors. Cell *139*, 61–72.

Wu, Y., Dissing-Olesen, L., MacVicar, B.A., and Stevens, B. (2015). Microglia: dynamic mediators of synapse development and plasticity. Trends Immunol. *36*, 605–613.

Cell Reports, Volume *23*

Supplemental Information

Sex-Specific Features of Microglia from Adult Mice

Alessandro Villa, Paolo Gelosa, Laura Castiglioni, Mauro Cimino, Nicoletta Rizzi, Giovanna Pepe, Federica Lolli, Elena Marcello, Luigi Sironi, Elisabetta Vegeto, and Adriana Maggi

Supplemental information

Supplemental Figures and Legends

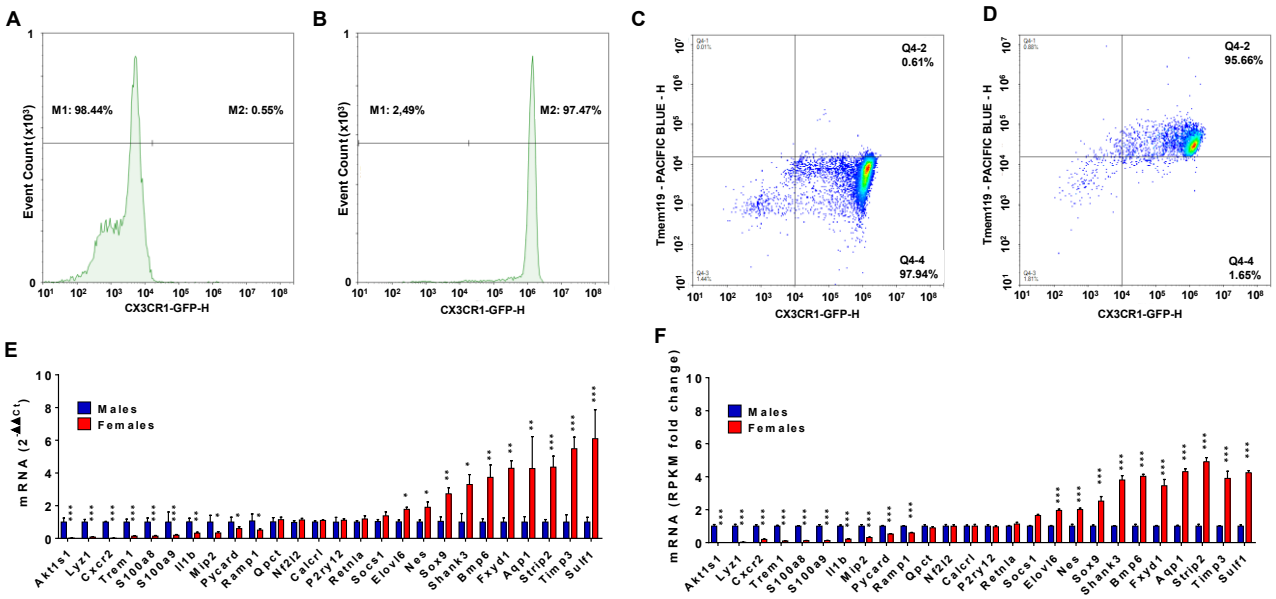

Figure S1. Validation of the methodologies. Related to Figure 1. Assessment of microglial purity after CD11b+ magnetic bead sorting by flow cytometry of GFP fluorescence in microglia isolated from the brain of wild type **(A)** or CX3CR1-GFP reporter **(B)** mice shows ~98% of GFP positive cells after microglia isolation. Density scatterplots of CX3CR1-GFP microglia incubated with isotype controls **(C)** or Tmem119-PacificBlue **(D)** show that GFP positive cells express the microglia specific marker Tmem119. Data are representative of three independent measures on n=3 individual animals/group. (**E**) qPCR validation: we selected a total of 26 genes (10 more expressed in males, 6 equally expressed and 10 more expressed in females). Data are expressed as $2^{-\Delta\Delta Ct}$ using the 36B4 transcript as an internal reference standard. Columns represent the mean ± s.e.m. of 6 animals per experimental group measured in triplicates. *, $P < 0.05$; **, $P < 0,01$; ***, $P < 0.001$ by one-way ANOVA and Tukey's method for multiple comparisons *versus* expression in male microglia (blue columns). The expression analyses made on the selected genes gave results superimposable with the results obtained by RNAseq (**F**).

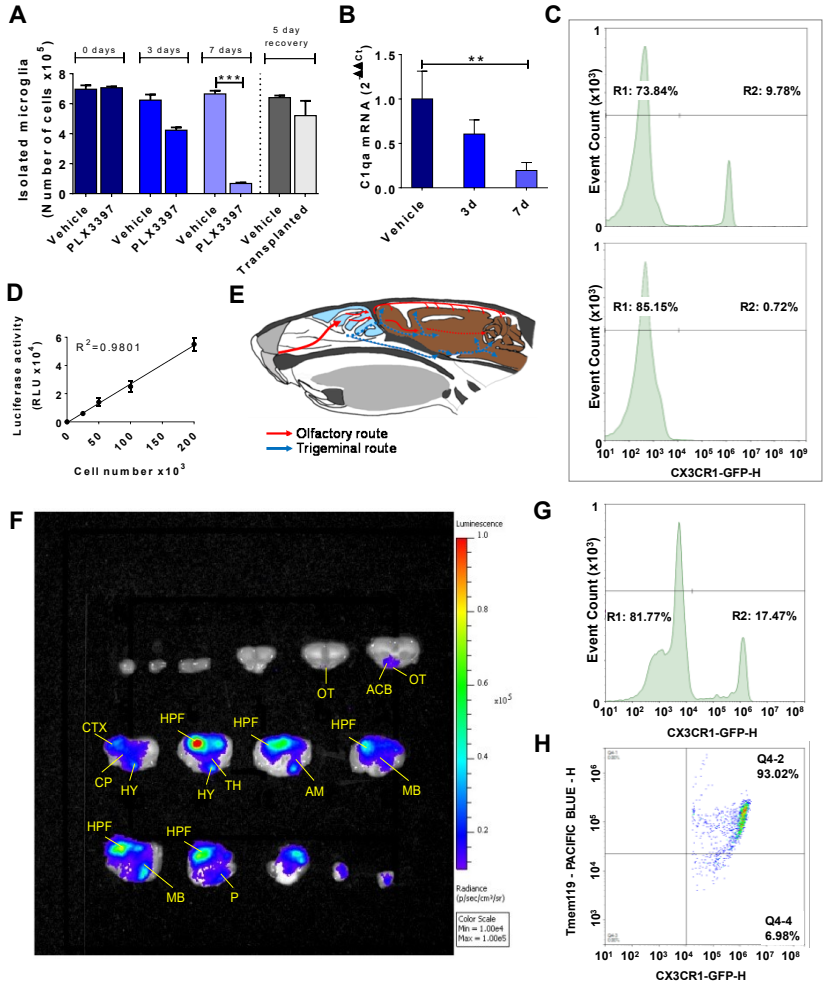

Figure S2. Female microglia retain their sex after transplantation in male brain. Related to Figure 3. Effect on microglia of PLX3397 administration in adult C57BL/6 mice was evaluated **(A)** by microglia isolation and counting; **(B)** by qPCR analyses of C1qa gene. Data are expressed as $2^{-\Delta\Delta Ct}$ using the 36B4 transcript as an internal reference standard. Columns represent the mean ± s.e.m. of 3 animals measured in triplicates. **, $P < 0.01$ by two-way; ***, $P < 0.001$ by two-way ANOVA *versus* expression in microglia isolated from vehicle-treated animals; (**C**) by flow cytometry (representative histogram of three independent measures on n=6 individual animals/group**)** of GFP fluorescence in the brain of CX3CR1-GFP reporter mice treated for 7 days with vehicle (upper panel) or PLX3397 (lower panel). **(D)** Luciferase activity measured in extracts of microglia isolated from male G4063 mice and expressed as relative luciferase units (RLU). Dots represent the mean ± s.e.m. of 3 independent measures on n=6 individual animals/group. *Brain colonization by transplanted microglia.* **(E)** Schematic drawing of two routes of transnasal delivery of cells to the brain. After crossing the cribriform plate, the olfactory route (red arrows) divides into two branches: (1) the CSF branch and (2) the parenchymal branch. Dashed arrows represent possible hypothetical routes of cell delivery. The hypothetical trigeminal route (blue arrows) consists of at least two branches one of which crosses the cribriform plate into the parenchyma, where it diverges to the rostral and caudal parts of the brain. The second branch projects from the nasal mucosa to the trigeminal ganglion, where the exogenously applied cells are further distributed to the forebrain and caudal brain areas including the brainstem and the cerebellum. **(F)** Identification of brain areas mainly enriched by transplanted bioluminescent microglia, according to Allen Mouse Brain Reference Atlas classification. Bioluminescence-based optical imaging of brain slices of WT male mice 5 days after transnasal administration of 400,000 bioluminescent microglial cells isolated from female G4063 mice; pseudocolors represent the intensity of light emission (p/s/cm2/sr). Brain areas have been identified according to Allen Mouse Brain Reference Atlas classification (http://www.brain-map.org/); OT: Olfactory Tubercle; ACB: Nucleus Accumbens; CTX: Cortex; CP: Caudoputamen; HY: Hypothalamus; Th: Thalamus; HPF: Hippocampal Formation; AM: Anteromedial Nucleus; MB: Midbrain; P: Pons. **(G)** Flow cytometry analyses of GFP fluorescence in microglia isolated from the brain of mice transplanted with CX3CR1-GFP microglia show ~18% of GFP positive cells (transplanted cells) after microglia isolation **(**histogram is representative of *n*=6 independent analyses**)**. R2-gated density scatterplots of CX3CR1-GFP microglia incubated with Tmem119-PacificBlue **(H)** show that GFP positive cells still express the microglia specific marker Tmem119. Histogram and scatterplot are representative of three independent measures on n=6 individual animals/group**)**.

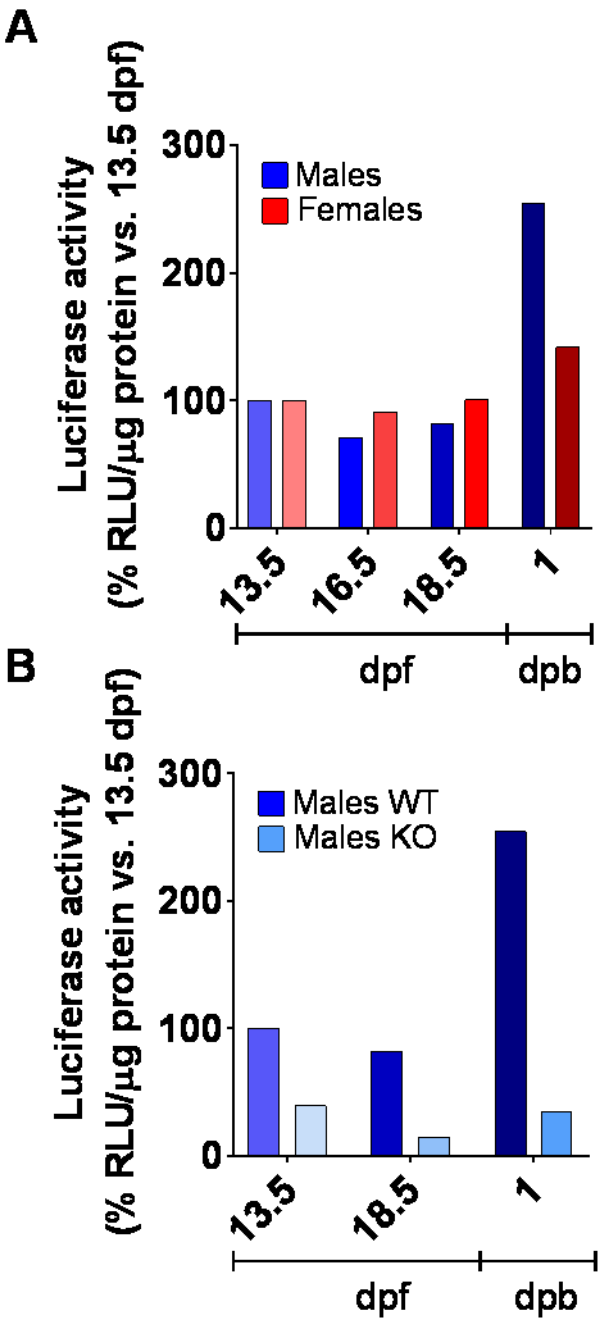

Figure S3. Luciferase expression in ERE-Luc mice shows that perinatal activation of ERα is restricted to male mice. Related to Figure 3. The ERE-Luc mouse was shown to selectively express luciferase under the control of intracellular estrogen receptors. **(A)** Quantitative analysis of luciferase expression in the brain of male and female ERE-Luc mice, shows that at postnatal day 1 (dpb) luciferase expression is significantly increased in the male, but not in the female brain; **(B)** quantitative analysis of luciferase in brain homogenates of male wild type (WT) or ERα KO (KO) ERE-Luc mice shows that the ERα is mainly responsible for the reporter expression. Each bar corresponds to relative luciferase units (RLU) representing the estrogen receptor activity vs. RLU measured at 13.5 dpf a) in male or female groups, or b) in male WT group.

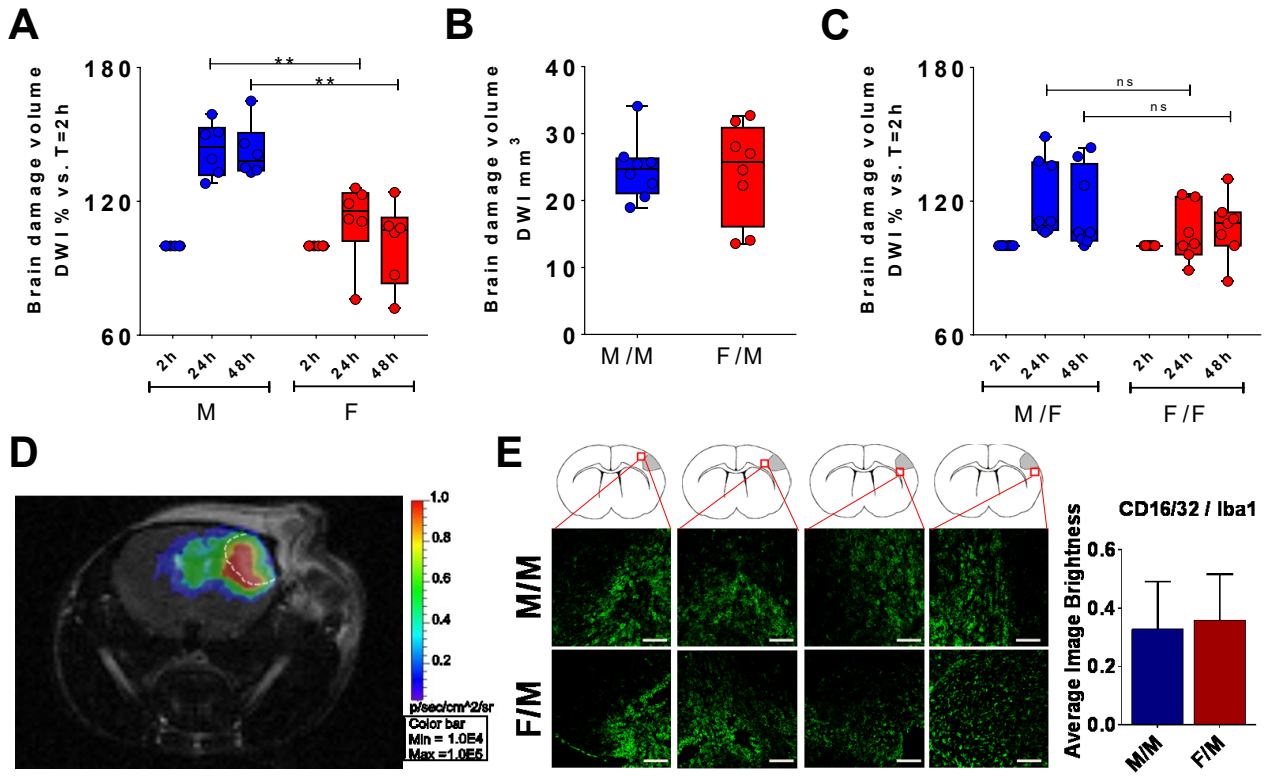

Figure S4. Protective action of female microglia in ischemia. Related to Figure 4. Scatter plot showing the quantitative analysis of the brain damage volume determined by DWI measurements and expressed as percent change relative to the initial 2 hours' value (**B**) set to 100%, in control **(A)** and transplanted female recipient **(C)** mice. Solid lines represent mean ± s.e.m. for *n*=6 (**A**), *n*=8 (**C**, M/F), *n*=7 (**C**, F/F). **, *P* <0.01; by two-way ANOVA and Sidak's method for multiple comparisons. ns= not statistically significant. **(D)** Representative image depicting the localization of transnasally-administered bioluminescent microglia 48h following pMCAO. The image was generated by the superimposition of bioluminescence imaging (in pseudocolors, representative of radiance (p/s/cm^2/sr)) and T2-weighted MRI collected in the same animal at a distance of -2.30 mm from the bregma**. (E)** Immunofluorescence analysis of coronal sections of brains excised from adult mice that had undergone pMCAO, stained for CD16/32. M/M: male recipient transplanted with male microglia; F/M: male recipient transplanted with female microglia. Images are representative of *n*=3 mice per experimental group, and report the observed fluorescence acquired in the areas indicated by red squares in the upper schematics. Scale bar: 10 µm. Graph columns show the mean ± s.e.m. of fluorescence brightness for CD16/32 (green channel) in Iba1 positive cells, measured in a double-blind manner in 20 fields per experimental group.

Supplemental Experimental Procedures

Animals and surgery

Animals were housed in the animal care facility of the Department of Pharmacological and Biomolecular Sciences at the University of Milan. To avoid the variability related to rearing, environment, or diets affecting the metabolism and the microbiome, both well-known regulators of the brain immune system (Hooper et al., 2012) care was taken to match the mice in terms of age, and to take the same numbers of males and females from each of the litters utilized in the study. To limit any circadian influence and facilitate the analysis of the phase of the cycle, in all experiments animals were euthanized at the same hours (between 2:00-4:00 p.m.); intact females were at metestrus, a phase with low circulating estrogens. The phase of the reproductive cycle in female mice was assessed by blind analysis of vaginal smears mounted on glass microscope slides and stained with May-Grünwald-Giemsa method (MGG Quick Stain Kit; Bio-Optica, Milan, Italy) according to the manufacturer's protocol. Animal groups for the RNA sequencing experiment were given an estrogen-free diet (AIN93M, Mucedola, Settimo Milanese, Italy) 2 weeks before and throughout the experiment. Ovariectomy (ovx) or sham surgery was performed under mild anesthesia obtained by *s.c.* injection of 50µl solution of ketamine (93.6 mg/kg, Ketavet 100; Intervet, Milan, Italy) and xylazine (7.2 mg/kg, Rompun; Bayer, Milan, Italy). At definite time points, animals were euthanized by intraperitoneal (*i.p.*) injection of lethal ketamine and xylazine solution (150 and 12 mg/kg, respectively).

Microglia sorting

Adult mice were transcardially perfused with ice-cold phosphate-buffer saline (PBS), brains were dissected and washed in Hank's Balanced Salt Solution (HBSS; Life Technologies); after removing the meninges, brains from six mice were pooled as a single experimental group. Enzymatic cell dissociation was performed using Neural Tissue Dissociation Kit P (Miltenyi Biotec, Bologna, Italy), following a modified version of the protocol supplied by the manufacturer. Briefly, after

enzymatic digestion with papain, samples were dissociated mechanically, homogenized, and filtered through a 40-μm cell strainer. After extensive washes in HBSS, myelin was removed by centrifuging the dissociated brain cells, which had previously been suspended in 10 ml of cold 0.9 M sucrose solution, at 850 g and 4°C for 10 min without braking. Floating myelin and the supernatant were discarded, and cells were processed for microglia magnetic sorting by incubating with CD11b MicroBeads (diluted 1:10 in PBS + 0.05% BSA; Miltenyi Biotec) for 15 min at 4°C; after washings, cells were suspended in 500 μl of PBS + 0.05% BSA and applied to a magnetic column to purify CD11b+ cells, namely microglia. Cell counting was performed using a TC20 Automated Cell Counter (BIORAD), according to the manufacturer's protocol. Immediately after isolation of microglia, cells were processed for subsequent analyses.

PLX3397 administration

For transnasal administration mice were placed in supine position, and a heated pad was inserted under the dorsal neck to induce a hyperextension of the head back. A total of 12 μl PLX3397 (100 μg) or vehicle solution (5% DMSO + 45% PEG300 + ddH2O) was given as nose drops (3μl/drop in each nostril corresponding to 6 μl/administration), alternating between the left and right nostrils for two times, at intervals of 2 min. Subsequent doses were given each 12 h, for 1 week.

RNA preparation

RNA was purified using RNeasy minikit protocol (QIAGEN, Milan, Italy), according to the manufacturer's instructions, including a step with deoxyribonuclease incubation. RNA Quality Control was performed on all RNA samples with an electrophoretic run on a Bioanalyzer instrument using the RNA 6000 Nano Kit (Agilent, Santa Clara, CA). RNA Integrity Number was determined for every sample and all the samples were considered suitable for processing based on the RNA integrity (RIN > 8). RNA concentration was estimated through spectrophotometric measurement using a Nanoquant Infinite M200 instrument (Tecan, Austria). Sequencing libraries

were prepared using the TruSeq™ RNA Sample Preparation Kit (Illumina, San Diego, CA) using 1.8 ug of total RNA as input. Polyadenylated transcripts were purified using poly-T oligo-attached magnetic beads. PolyA RNA was fragmented at 94°C per 8 minutes and retrotranscribed using random hexamers. Multiple indexing adapters were ligated to the ends of the ds cDNA and the amount of DNA in the library was amplified with 10 PCR cycles. Final libraries were validated and quantified with the DNA1000 kit on the Agilent Bioanalyzer Instrument. Pooled libraries were sequenced on the Illumina Genome Analyzer II_x producing an average of 13 M reads per library.

Real time PCR

One µg RNA were used for cDNA preparation using 8 U/µl of Moloney murine leukemia virus reverse transcriptase (Promega, Milan, Italy) in a final volume of 25 µl; the reaction was performed at 37°C for 1 h, and the enzyme inactivated at 75°C for 5 min. Control reactions without the addition of the reverse transcription enzyme were performed (data not shown). A 1:4 cDNA dilution was amplified using GoTaq®qPCR Master Mix technology (Promega) according to the manufacturer's protocol. The PCR was carried out in triplicate on a 96-well plate using 7900HT fast real time PCR system (Applied Biosystems, Life Technologies) with the following thermal profile: 2 min at 95°C; 40 cycles, 15 sec at 95°C, 1 min at 60°C. Data were analyzed using the $2^{-\Delta\Delta Ct}$ method.

Bioinformatic analysis

BaseCall files were converted to FastQ files using Casava 1.8.2. Sequencing reads were aligned to the mouse genome (mm10) using TopHat v.2.0.9. Transcripts were reconstructed and quantified using Cufflinks v2.1.1 and differential expression analysis was performed using CuffDiff Trapnell, 2012)[31]. Cuffdiff uses the test statistics T = E[log(y)]/Var[log(y)], where y is the ratio of the normalized counts between two conditions. Overrepresentation analysis (ORA) on DEG lists was performed using the Functional Annotation Tool in DAVID website (https://david.ncifcrf.gov/*) and*

Enrichr for enrichment analysis. The mouse genome was used as background list. Biological processes, molecular functions and KEGG pathways were investigated focusing on enriched terms with a Benjamini adjusted p-value less than 0.05. Transcription Factors potentially involved in the regulation of DEG were identified using the "ENCODE and ChEA Consensus TFs from ChIP-X" database. Heatmaps and hierarchical clustering have been obtained using Genesis software.

Primer list

All mouse: *Xist* forward 5′- CTATCGCCCCAGGTCACATC-3′; *Xist* reverse, 5′-CCAGTGCAGAGGTTTTTGGC-3′; *C1qa* forward 5′-GACCACGGAGGCAGGGACAC-3′; *C1qa* reverse 5′-CTTCCCGTTGGGTGCTCGGC-3′; *Ki67* forward 5′-AGAGCTAACTTGCGCTGACT-3′; *Ki67* reverse 5′-GTTGTTCCCTGAGCAACACTG-3′; *Cdk3* forward 5′-TGCTCGCACTTGGCTTCAAA-3′; *Cdk3* reverse 5′-GGTATGGTAGATCCCGGCTTATT-3′; *Akt1s1* forward 5′- GGACGAGCCCACTGAAACA-3′; *Akt1s1* reverse, 5′-CTGCCGTCGTCTGTGCTCT-3′; *Trem1* forward 5′- GTGTATCCAGCCCTCACAACT-3′; *Trem1* reverse 5′-GAAGCCAAGGTGAGGAGTCC-3′; *S100a9* forward 5′-AGTGTCCTCAGTTTGTGCAGAATA-3′; *S100a9* reverse 5′-TGAGATGCCACACCCACTTT-3′; *Cxcl2* forward 5′- TGAACAAAGGCAAGGCTAACTGACC-3′; *Cxcl2* reverse 5′-ACGATCCAGGCTTCCCGGGTG-3′; *Shank3* forward 5′- GTGACCAGGAAACCCGAGG-3′; *Shank3* reverse, 5′-AACTTCTCCCCTTTTCTTCTCCG-3′; *Fxyd1* forward 5′-GGGGTCCAAAGTGCTTAGCT-3′; *Fxyd1* reverse 5′-CGCAGGGTGTGGTAATCGTA-3′; *Aqp1* forward 5′- CCTGCTGGCGATTGACTACA-3′; *Aqp1* reverse 5′-TGGTTTGAGAAGTTGCGGGT-3′; *Timp3* forward 5′- GGCCTCAATTACCGCTACCA-3′; *Timp3* reverse 5′-ATGCAGGCGTAGTGTTTGGA-3′; *Il1β* forward 5′- TGCCACCTTTTGACAGTGATG-3′; *Il1β* reverse 5′-GCTGCGAGATTTGAAGCTGG-3′; *Iba1* forward 5′-ACCCAGCGGACAGACTGCCA-3′; *Iba1* reverse 5′-TTTCCTCCCTGCAAATCCCTGCT-3′; *36b4* forward 5′- GGCGACCTGGAAGTCCAACT-3′; *36b4* reverse 5′-

CCATCAGCACCACAGCCTTC-3′. Amplification efficiencies for each target gene are comparable.

Ex vivo imaging

Mice were injected i.p. with 80 mg/kg of luciferin (Beetle Luciferin Potassium Salt; Promega, Madison, WI, USA) 15 min prior euthanasia and subjected to *ex vivo* imaging immediately after death. Brains were rapidly dissected and sectioned by means of a brain matrix (adult mouse, coronal and, 1 mm spacing; Ted Pella, Redding, CA). Imaging analysis was carried out with a CCD-camera (IVIS Lumina II Quantitative Fluorescent and Bioluminescent Imaging; PerkinElmer, Waltham, MA, USA) using 5 min exposures. Photon emission was quantified with the Living Image Software (PerkinElmer).

Luciferase enzymatic assay

Organs or cells were homogenized in Reporter Lysis Buffer (Promega, Italy) and lysates were subjected to three cycles of freezing and thawing. Proteins were separated from DNA and lysosomes by centrifugation (13000 × g for 30min), after having measured the protein concentration of the extract by the Bradford assays, the biochemical assay of Luciferase activity was carried out with a luciferase assay buffer (470 μM luciferine, 20 mM Tricine, 0.1 mM EDTA, 1.07 mM (MgCO3)4·Mg(OH)2 × 5H2O; 2.67 mM MgSO4 × 7H2O in H2O, pH 7.8, with 33.3 mm DTT and 530 μM ATP) by measuring luminescence emission with a luminometer. The relative luminescence units (RLU) determined during a measurement of 10 s time was expressed as RLU per microgram protein. As background, RLU were measured in the same organs or cells derived from WT mice. The RLU measured in WT mice were routinely subtracted from the RLU measured in the TG mice.

Magnetic Resonance Imaging Analysis

Mice were anesthetized with isofluorane (2% for induction, 1% for maintenance) in 1 L/min of O_2, fixed on the holder and placed into the 6.4 cm diameter birdcage coil. A 3-orthogonal-plane, gradient echo scout acted as a geometric reference for locating the olfactory bulb. Three different DWIs were acquired using 3 orthogonal diffusion gradient directions; the reference images were identical but without diffusion gradients. Acquisition parameters were: repetition time (TR) = 1500 ms, effective echo time (TE) = 40 ms, number of averages (NA) = 8, matrix resolution = 128 x 128, slice thickness = 0.8 mm, interslice distance = 1 mm and number of contiguous slices = 10.

One week after MCAO, T2-Weighted images were obtained with a RARE sequence with the following parameters: TE = 80 ms, a TR = 3 sec, refocusing flip angle = 180°, FOV = 4.0x4.0 cm^2, matrix resolution = 128x128, slice thickness = 0.8 mm, interslice distance = 1 mm and number of contiguous slices = 16. Twelve signal averages were recorded for a total scan time of 4 min and 48 sec. Lesions were identified as areas of high signal intensity.

Immunocytochemistry

Cells were fixed with 4% Paraformaldehyde (PFA)-4% sucrose in PBS solution at 4 °C and washed several times with PBS. Cells were permeabilized with 0.1% Triton X-100 in PBS for 10 min at room temperature and then blocked with 5% BSA in PBS for 30 min at room temperature. Cells were then labelled with anti-Iba1 rabbit antibody (1:1000; Wako) overnight at 4 °C. Cells were washed and then incubated with goat anti-rabbit secondary antibody conjugated with Alexa Fluor 594 (1:200; Life Technologies, Italy) for 1 h at room temperature. Cells were then washed in PBS and mounted on glass slides with Fluoromount mounting medium (Sigma Aldrich).

Immunofluorescence analysis

One week after MCAO, transplanted mice were perfused with phosphate-buffered saline (PBS) and then 4% paraformaldehyde in PBS for at least 25 minutes. Brains were then removed, post-fixed 1 hour in 4% paraformaldehyde and cryoprotected in 30% sucrose solution until precipitation at 4°C.

Briefly, coronal sections of 20-µm were incubated overnight at 4°C with the primary rabbit antibody anti-Iba1 (1:30,000; Biocare Medical., USA) in PBS plus 5% normal goat serum (Dako, Denmark) and 0.1% Triton-X 100. The signal intensity was enhanced using the High Sensitivity Tyramide Signal Amplification kit and fluorescent SA-Cyanine 5 (TSA PLUS Biotin KIT; Perkin-Elmer, Italy) and Alexa Fluor 633-conjugated streptavidin (1:2,000; Life Technologies, Italy), following the manufacturer's instructions. The sections were then incubated overnight at 4°C with the primary rabbit antibody anti-YM1 (1:100; StemCell Technologies, USA) and exposed for 2 hours at room temperature to goat anti-rabbit secondary antibody conjugated with Alexa Fluor 555 (1:600; Life Technologies, Italy). Nuclei were labeled with Hoechst 33258 (0.3 µg/ml; Life Technologies, Italy). For the quantitative analysis, we selected four fields of view (FOVs; 562.50 µm x 562.50 µm) surrounding the ischemic lesion, as illustrated in the drawing (Fig. 4C). Images were acquired using a confocal microscope at 20x magnification (merge of 8-µm z-stack at 2-µm intervals) or 100x magnification (merge of 12-µm z-stack at 0.5-µm intervals, LSM510 META, Zeiss, Germany). Mean gray values of each channel were measured using ImageJ in a double-blind manner, in order to obtain a semi-quantitative evaluation of the expression of each marker.

FACS cytometry

Cell sorting experiments were performed on at least 500.000 cells for each sample by using MoFlo Astrios instrument (Beckman Coulter) equipped with 488, 546 and 640 nm lasers. For Tmem119 detection, cells were incubated 30 minutes at 4°C with Anti-TMEM119 rabbit antibody (1:500, Abcam), washed and incubated 30 minutes at 4°C with goat anti-rabbit secondary antibody conjugated with Pacific Blue (1:500, Life Technologies, Italy). Fluorescence pulses were detected using a band pass filter 531/26 nm for GFP, and 450/50 nm for Pacific Blue. Results were analyzed using Kaluza software (Beckman Coulter).